Digital Mammography: Gabor Filters for Detection of Microcalcifications

Barbara Caputo[1,*] and Giovanni E. Gigante[2]

[1]University of Erlangen, Chair for Pattern Recognition,
Martensstrasse 3, D-91058, Erlangen, Germany
e-mail: caputo@informatik.uni-erlangen.de
[2]University of Rome "La Sapienza", Physics Department - CISB,
Piazza A. Moro 3, 00161 Rome, Italy
e-mail: gigante@caspur.it

To appear in Proceeding of Vision, Modeling and Visualization 2000, Germany

Abstract

Mammography associated with clinical breast examination is the only effective method for mass breast screening. Microcalcifications are one of the primary signs for early detection of breast cancer. Texture-analysis is a very popular method proposed in literature for detecting clustered microcalcifications in digitized mammograms. In this paper [1] we propose Gabor Filters for classification of difficult-to-diagnose regions in mammographic images. Textural features extracted by this method are used for the classification of positive Region of Interest (ROI's) containing clustered microcalcifications and negative ROI's containing normal tissue. A three-layer back-propagation neural network is used as a classifier, and a Receiver Operating-Characteristics (ROC) analysis is used to evaluate the classification performance. The obtained results show that Gabor Filters can be successfully employed for detection of microcalcifications.

[1]This research work was developed while B. Caputo was at the University of Rome "La Sapienza", as partial fulfilment of her laurea degree; the * indicates the corresponding author

1 Introduction

Screen-film mammography associated with clinical breast examination and breast self-examination is widely recognized as the only effective imaging modality for early detection of breast cancer in women [1], [2]. However, the interpretation of X-ray mammograms is very difficult because of the small differences in the image densities of various breast tissues, particularly for dense breast. The interpretation of mammograms by radiologists is performed by a visual examination of films for the presence of abnormalities that indicate cancerous changes. Computerized analysis to help decision making for biopsy recommendation, and diagnosis of breast cancer might be of significant value to improve the true-positive rate of breast cancer detection. Among the early indicators of breast cancer, microcalcifications are one of the primary signs [2]. They are tiny granule-like depositum of calcium, and the presence of clustered microcalcifications in X-ray mammograms is considered a basical marker for the early detection of breast cancer, especially for individual microcalcifications with diameters up to about $0.7mm$ and with an average diameter of $0.3mm$ [2]. Computerized image analysis methods have been used for the identification of circumscribed masses, classification of suspicious areas and classification of microcalcifications using conventional methods [3], [4] and using expert systems [3]. In the actual interpretation of mammographic microcalcifications, the grey-level values defining local structures in the microcalcification clusters play a significant role [2]. It has been demonstrated in clinical studies described in [2], that the grouping of microcalcification regions, in order to define the shape of the cluster, is highly dependent on the gray-level-based structure and texture of the image. Texture information plays an important role in image analysis and understanding, with potential applications in remote sensing, quality control, and medical diagnosis. Texture is one of the important characteristics used in identifying an object or a region of interest (ROI) in an image [5].

In this paper we propose Gabor Energy Filters (GEFs) for microcalcifications detection; Gabor functions have been introduced by Gabor in 1946 [6], and have been later extended to 2D [7]; by applying arguments from quantum mechanics, Gabor demonstrated that this class of functions is optimal in the sense that it possesses the smallest product of spatial extent by effective frequency width. This property suggested that these filters are appropriate operators for tasks requiring simultaneous measurements in these domains, such as texture discrimination. This technique has been applied successfully in many texture analysis and segmentation problems [8], [9], [10], [11]. Textural features extracted with GEFs were used to classify Region Of Interests (ROI's) into positive ROI's containing microcalcifications and negative ROIs containing normal tissues. A feedforward, three-layer backpropagation neural network was employed as a classifier [12]; a Receiver Operating-Characteristics (ROC) analysis [13] was used to evaluate the classification performance of the GEFs.

The paper is organized as follows: Gabor Functions and GEFs are described in Section 2. The experimental results are presented in Section 3; the three-layer backpropagation neural network used as classifier is also described in Section 3. Finally, conclusions are given in Section 4.

2 Gabor Functions and Gabor Filters

The Fourier Transform (FT) of a function $f(x)$ gives a measure of its irregularities (high frequencies), but this information is not spatially localized. For localizing the information obtained by the FT, Gabor [6] defined a new decomposition using a Gaussian window in the Fourier integral. These functions have been later extended to 2-D by Daugman [7], [14]. A Gabor Function is given by

$$h(x,y) = g(x',y')\exp[2\pi j(Ux+Vy)], \quad (1)$$

with

$$(x',y') = (x\cos\theta + y\sin\theta, -x\sin\theta + y\cos\theta).$$

They are rotated spatial- domain coordinates; (u,v) denote frequency-domain coordinates, and (U,V) represent a particular 2-D frequency [15]. The complex exponential is a 2-D complex sinusoid at frequency

$$\omega = \sqrt{U^2+V^2}$$

and

$$\Phi = \arctan(V/U);$$

it specifies the orientation of the sinusoid. The function $g(x,y)$ is the 2-D Gaussian

$$g(x,y) = \frac{1}{2\pi\sigma_x\sigma_y}\cdot$$

$$\exp\left\{-\frac{1}{2}\left[\left(\frac{x}{\sigma_x}\right)^2 + \left(\frac{y}{\sigma_y}\right)^2\right]\right\}, \quad (2)$$

where σ_x and σ_y are related with the spatial extent and bandwidth of the filter. The Gabor function can thus be viewed as a Gaussian modulated by a complex sinusoid. It is possible to demonstrate that the Fourier Transform of $h(x,y)$ is

$$H(u,v) =$$

$$\exp\left\{-\frac{1}{2}[(\sigma_x[u-U]')^2 + (\sigma_y[v-V]')^2]\right\}, \quad (3)$$

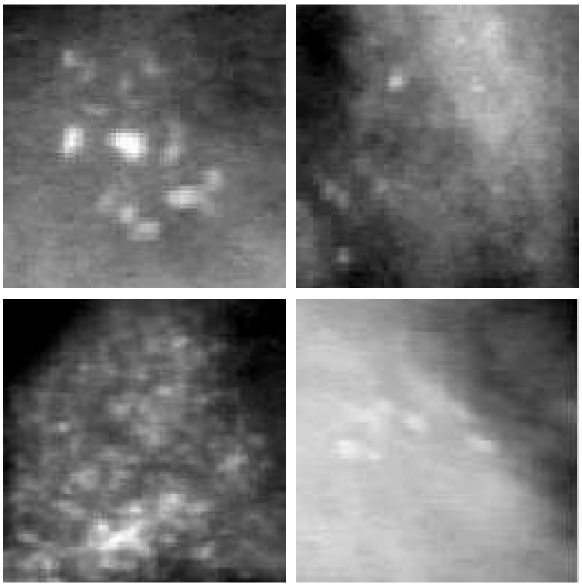

Figure 1: Four examples of ROIs containing microcalcifications.

where

$$(u-U)^{'} = (u-U)\cos\theta + (v-V)\sin\theta,$$
$$(v-V)^{'} = -(u-U)\sin\theta + (v-V)\cos\theta.$$

This means that the frequency response of the Gabor Function has the shape of a Gaussian; its major and minor axis width will be determined by σ_x and σ_y, it will be rotated by an angle θ with respect to the u-axis, and it will be centered about the frequency (U, V). Thus, the Gabor functions can be viewed as band-pass filters. In this paper we will assume that $\sigma_x = \sigma_y = \sigma$. This means that the parameter θ is not needed and the Gabor Function becomes:

$$h(x,y) = \frac{1}{2\pi\sigma^2}\exp\left\{-\frac{(x^2+y^2)}{2\sigma^2}\right\}\cdot \exp[2\pi j(Ux+Vy)]. \quad (4)$$

We can define now the Gabor Filter G_h:

$$G_h(I(x,y)) = |I(x,y) * h(x,y)|, \quad (5)$$

where $I(x,y)$ is an image.

2.1 Gabor Filters for Texture Analysis

Gabor Filters applied to texture analysis measure the similarity between neighbourhoods in an image and Gabor functions. A family of Gabor functions can be generated for varying frequencies (ω) and Gaussian window standard deviations (σ); remembering that

$$\omega = \sqrt{U^2+V^2},$$
$$\Phi = \arctan(V/U)$$

and expressing (U, V) by means of the orientation θ [15], we can write the Gabor function as

$$G(x,y|\lambda,\theta,\phi,x_0,y_0) = \exp^{-\frac{[(x-x_0)^2+(y-y_0)^2]}{2\sigma^2}}\cdot \sin(\frac{2\pi}{\lambda}(x\cos\theta - y\sin\theta)+\phi), \quad (6)$$

where (x_0, y_0) specify the center of the Gaussian.

For texture analysis purpose, we'll compute the GEF at each pixel for each combination of wavelength and orientation, where the energy is defined as the sum over the phases of the squared filter values. That is

$$S^2(x_0,y_0|\lambda,\theta) = \left[\sum_{x,y} G(x,y|\lambda,\theta,0,x_0,y_0)I(x,y)\right]^2 + \left[\sum_{x,y} G(x,y\lambda,\theta,\pi/2,x_0,y_0)I(x,y)\right]^2. \quad (7)$$

Energy calculated using eq.(7) for each combination of λ and θ may be used as textural features [16].

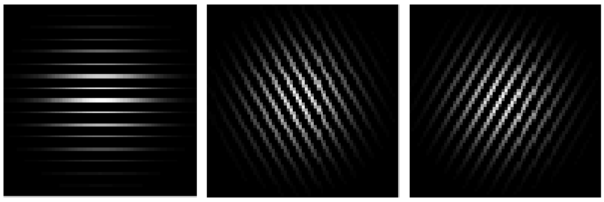

Figure 2: GEFs for $\lambda = 4$, $\theta = 0, \pi/3, 2\pi/3$

3 Experimental Results

3.1 Data Selection

We tested the performance of GEFs for microcalcifications detection on a database of 81

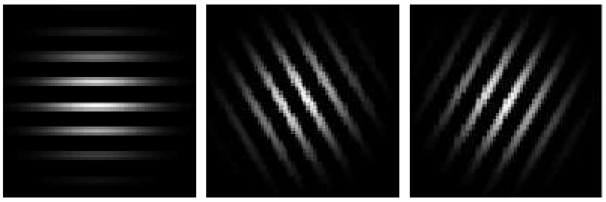

Figure 3: GFEs for $\lambda = 8$, $\theta = 0, \pi/3, 2\pi/3$

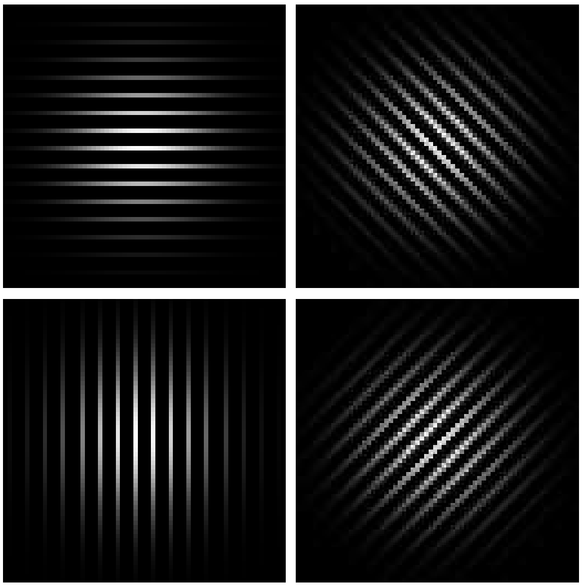

Figure 4: GEFs for $\lambda = 4$, $\theta = 0, \pi/4, \pi/2, 3\pi/4$

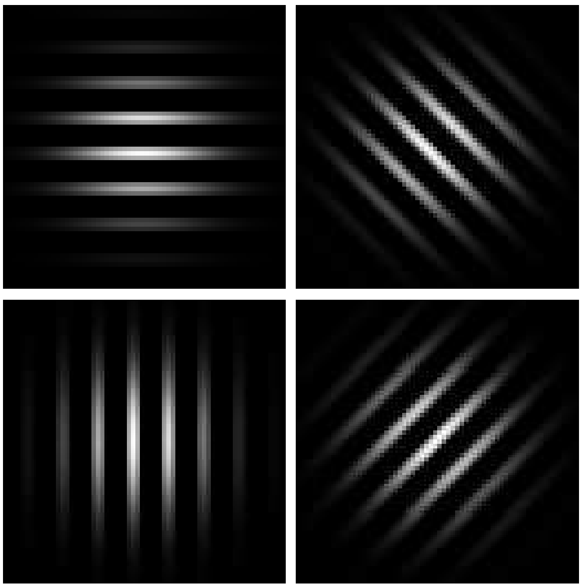

Figure 5: GEFs for $\lambda = 8$, $\theta = 0, \pi/4, \pi/2, 3\pi/4$

Layers Number	3
Hidden Neurons	10
Output Neurons	1
Transfer Function	Log-sigmoid
Learning Rule	backpropagation
error goal	0.1

Table 1: Network architecture and learning parameters

	GFE192	GFE256
λ(pixels)	32, 16, 8, 4	32, 16, 8, 4
θ(rad)	$\pi/3, 2\pi/3, \pi$	$\pi/4, \pi/2, 3\pi/4, \pi$
x_0(pixels)	16, 48, 80, 112	16, 48, 80, 112
y_0(pixels)	16, 48, 80, 112	16, 48, 80, 112

Table 2: Parameters of GEF192 and GEF256

images produced by the "Centro per la Cura e la prevenzione dei Tumori" of the University of Rome "La Sapienza"; each image was digitized from film using a CCD camera operating at a spatial resolution of 604×575 pixels for image; the pixel rate was of $11,5MHz$, and the pixel size of $10\mu m \times 15\mu m$. From the 81 images, 151 Region of Interest (ROI) were selected by expert radiologists, each of 128×128 pixels. Among the selected 151 ROIs, 75 were positive and 76 were negative; four different ROIs are shown in Figure 1. In a preprocessing step, each extracted ROI was stretched to the normalized gray-level range of 0-255 [5].

3.2 Feature Extraction

As shown in Section 2, a GEF set is specified by the values of the parameters $\lambda, \theta, x_0, y_0$. In this paper we used two filter sets: 4 frequencies (wavelengths of 32,16, 8 and 4 pixels), 16 centers of the Gaussian ($x_0 = y_0 = 16$, 48, 80, 112 pixels) and two different possible choices for θ: $\theta = 0^0, 45^0, 90^0, 135^0$ and $\theta = 0^0, 60^0, 120^0$. So, in the first case we had 192 coefficients (we'll call this set GEF192), and in the other case 256 coefficients (GEF256). These value parameters are summarized in Table 2.

3.3 Classifier

An artificial neural network is a computer architecture consisting of a single interconnected processing elements called neurons [13], [17], [18]. A weight w_{ij} (coupling strength) characterizes the interconnections between any two neurons i and j. The input to each neuron is a weighted sum of the outputs incoming from the connected neurons. Each neuron operates on the input signal using his activation function f and produces the output response. The typical activation functions are linear, threshold and sigmoid [17], [18]. Normally the neurons are organized in an architecture with input nodes, interfacing the neural network and the external world, output nodes, producing the network's responses, and hidden nodes, having the task of correlating and building up an "internal representation" of the analyzed problem. Network's capacity and performance depends on the number of neurons, on the activation functions used, and on the neurons' interconnections. Another important attribute of artificial neural networks is that they can efficiently learn nonlinear mappings through examples contained in a training set, and use the learned mapping for complex decision making [17], [18].

A three-layer, backpropagation neural network was employed as classifier in this research. In Table 1 are summarized the network architecture and the learning parameters; the initial weights are randomly selected from $[0.0, 1.0]$. The textural features extracted by means of GEFs, as described in section 3.2, are used as the input signals of the input layer. There is a single output node for classification into positive or negative ROI. A non-linear sigmoid function with zero and one saturation values is used as the activation function for each neuron, and is defined as [13]

$$o_j = \frac{1}{1 + e^{\sum_i w_{ij} o_i + v_j}} \tag{8}$$

where o_j is the output of the j-th neuron and v_j is the threshold value of the j-th neuron. The network is trained to provide a 1.0 output value for a positive ROI and a 0.0 output value for a negative ROI. In the training process, the weights between the neurons are adjusted iteratively so that the differences between the output values and the target values are minimized. In this study, the training process is stopped when the error per training case becomes smaller than 0.1.

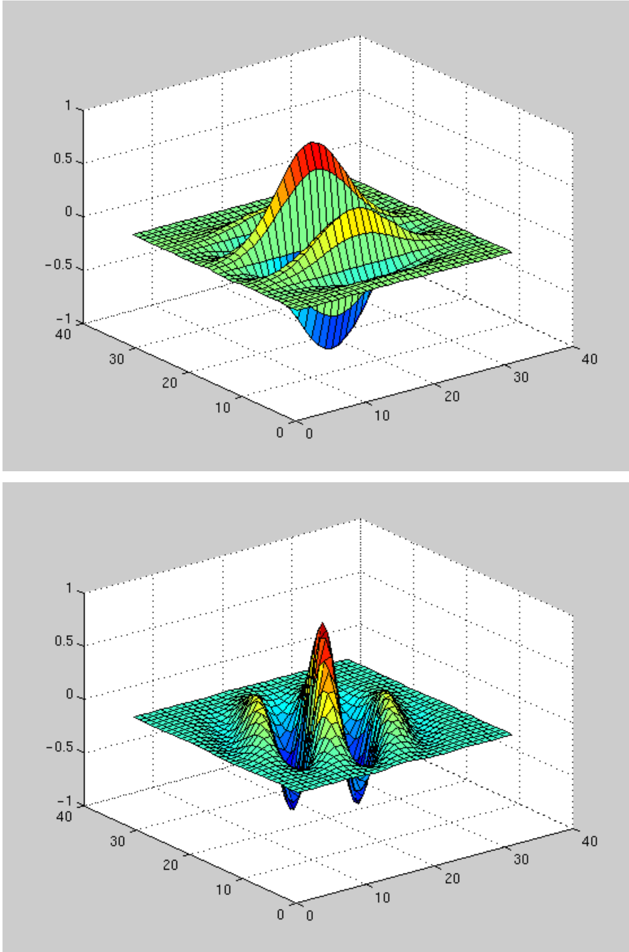

Figure 6: Two examples of 2D Gabor functions.

3.4 Classification Results

The two sets of textural features obtained using the GEFs as described in section 3.2 were used as input for the network described in section 3.3. We used three different combinations of training and test sets: 40 training cases and 111 test cases for the *set*1, 50 training cases and 105 test cases for the *set*2, and 60 training cases and 95 test cases for the *set*3. For every set, we randomly chose 10 different partitions of the data; this procedure should prevent a dependency of the results on a particular partitioning of the data. The results of the network for all the different partitions were analysed by using ROC analysis [5]. ROC analysis is based on statistical decision theory and has been applied extensively to the evaluation of clinical diagnosis. The ROC curve represents the relationship between the true-positive fraction (TPF) and the false-positive fraction (FPF) for variation of the decision threshold. The TPF and the FPF denote the fraction of patient actually having the disease in question that are diagnosed as positive and the fraction of patients actually without the disease in question that are diagnosed as positive, respectively. The area under the ROC curve A_z is used as a measure of the classification performance. A higher A_z indicates better classification performance because a larger value of TPF is achieved at each value of FTF. An ideal performance produces an area of 1.0.

ROC analysis was applied on the classification results obtained for $set1$, $set2$ and $set3$, for each of the 10 different partitions of the data. In this way 10 different values of A_z, for each set, were obtained: the average A_z obtained for $set1$ has been of 0.79 for GEF192 and of 0.84 for GEF256; the average A_z obtained for $set2$ has been of 0.83 for GEF192 and of 0.87 for GEF256; the average A_z obtained for $set3$ has been of 0.84 for GEF192 and of 0.89 for GEF256. These results are summarized in Table 3.

The better performance achieved by both the feature sets with $set3$ indicates that the network has generalized better with the bigger training set; for every data partition, the best results were obtained with the GEF256 representation.

	GEF192	GEF256
$A_z(set1)$	0.79	0.84
$A_z(set2)$	0.83	0.87
$A_z(set3)$	0.84	0.89

Table 3: Classification results.

4 Conclusion

In this paper we proposed GFs for detection of microcalcifications in mammographic images. The extracted features constituted the input of a neural network trained to classify between ROI's containing microcalcifications and ROI's containing normal tissue. The performance of the network was evaluated by means of a ROC analysis. The obtained results show the effectiveness of this approach; future work will compare this method with others already used in literature, such as Wavelet Transform and statistical methods.

Acknowledgments

We would like to thank Prof. V.Virno and the staff of the Radiology Department of the "Centro per la Cura e la Prevenzione dei Tumori" of the University of Rome "La Sapienza" for their cooperation.

References

[1] E. A. Sickles and D. B. Kopans, "Mammographic screening for women aged 40 to 49 years: the primary practitioner's dilemma", *Anna. Intern. Med.*, vol. 122, no. 7, pp. 534-538, 1995.

[2] M. Lanyi, "*Diagnosis and Differential Diagnosis of Breast Calcifications*", New York: Springer-Verlag, 1986.

[3] S. Morio and S. Kawahara et al., "Expert system for early detection of cancer of the breast", *Comp. Biol. Med.*, vol. 19, no. 5, pp. 295-305, 1989.

[4] L.Shen, R. M. Rangayyan and J. E. L. Desautels, "Application of shape analysis to mammographic calcifications", *IEEE Trans. Med Imag.*, vol. 13, no. 2, pp. 263-274, 1994.

[5] A. K. Jain, "*Fundamental of digital image processing*", Prentice Hall, Englewood Cliffs, 1989.

[6] D. Gabor, “Theory of communication”, *J. Inst. Elect. Eng.*, London, vol. 93, pp. 429-457, 1946.

[7] J. D. Daugman, “Two-dimensional spectral analysis of cortical receptive field profiles”, *Vision Res.*, vol. 20, pp. 847-856, 1980.

[8] A. C. Bovik, M. Clark and W. S. Geisler, “Mulichannel texture analysis using localized spatial filters”, *IEEE Trans. Pattern Analysis and Machine Intelligence*, vol. 12, pp. 55-73, Jan 1990.

[9] A. K. Jain and F. Farrokhnia “Unsupervised texutre segmentation using Gabor Filters”, *Pattern Recognition*, vol. 24, no. 12, pp. 1167-1186, 1991.

[10] B. Caputo, *Morphological analysis of biomedical images with space-frequency techniques and neural networks*, Laurea thesis (in italian), University of Rome “La Sapienza”, 1998.

[11] B. Caputo, P. Lanucara, G. E. Gigante, “Morphological analysis of mammographic images with Gabor transform and neural networks”, *proc. of ICIAM99*, Edimburgh, July 5-9, 1999.

[12] C. E. Metz, “ROC methodology in radiologic imaging”, *Investigate Radiology*, vol. 21, no. 9, pp. 720-733, 1986.

[13] R. P. Lippmann, “An introduction to computing with neural nets”, *IEEE ASSP Magazine*, pp. 4-22, April 1987.

[14] J. D. Daugman, “Uncertainty relation for resolution in space, spatial frequency and orientation optimized by two-dimensional visual cortical filters”, *J. Opt. Soc. Amer. A*, vol. 2, pp. 1160-1169, July 1985.

[15] D.Dunn, W. Higgins and J. Wakeley, “Texture segmentation using 2-D Gabor elementary functions”, *IEEE Trans. Patt. Anal. Machine Intell.*, vol. 16, pp. 130-149, Feb. 1994.

[16] I. Fogel and D. Sagi “Gabor filters as texture discriminator”, *Journal of Biological Cybernetics*, vol. 61, pp. 103-113, 1989.

[17] D. E. Rumelhart and C.R. Rosemberg, *Parallel Distributed Processing*, the MIT Press, Cambridge MA, 1986.

[18] C. M. Bishop, *Neural Networks for Pattern Recognition*, Claredon Press - Oxford, 1995.